Real-time evolution and quantized charge pumping in magnetic Weyl semimetals

Takahiro Misawa,[1] Ryota Nakai,[2] and Kentaro Nomura[2,3]
[1]*Institute for Solid State Physics, University of Tokyo, 5-1-5 Kashiwanoha, Kashiwa, Chiba 277-8581, Japan*
[2]*Institute for Materials Research, Tohoku University, Sendai 980-8577, Japan*
[3]*Center for Spintronics Research Network, Tohoku University, Sendai, 980-8577, Japan*

(Received 17 July 2019; published 14 October 2019)

Real-time evolution and charge pumping in magnetic Weyl semimetals are studied by solving the time-dependent Schrödinger equations. In the adiabatic limit of the real-time evolution, we show that the total pumped charge is quantized in the magnetic Weyl semimetals as in the quantum Hall system, although the Weyl semimetal has no bulk gap. We examine how the disorder affects the charge pumping. As a result, we show that the quantized pumped charge is robust against the small disorder and find that the pumped charge increases in the intermediate disorder region. We also examine the doping effects on the charge pumping and show that the remnant of the quantized pumped charge at zero doping can be detected. Our results show that the real-time evolution is a useful technique for detecting the topological properties of the systems with no bulk gap and/or disorders.

DOI: 10.1103/PhysRevB.100.155123

I. INTRODUCTION

Immediately after the discovery of the integer quantum Hall effects [1], Laughlin presented the simple and important gedanken experiment for explaining the quantized Hall conductivity [2]. In Laughlin's gedanken experiment, by adiabatically introducing the magnetic flux Φ from zero to $\Phi = \Phi_0 = e/h$ into the quantum Hall system on a cylinder, the electrons move from one edge to the opposite side of the edge as schematically shown in Fig. 1. Due to the invariance of the wave functions under the gauge transformation by the flux Φ, it is shown that the total pumped charge should be quantized when $\Phi = \Phi_0$.

In a similar way, Thouless argued the charge pumping in one-dimensional systems with slow time-dependent periodic potentials [3]. By solving the time-dependent Schrödinger equations, Thouless showed that the pumped charge is quantized and it is related to the topological invariant. The charge pumping caused by introducing the external flux is called the *Thouless pumping*, and Laughlin's argument can be regarded as the adiabatic limit of the Thouless pumping. Although the realization of the Thouless pumping in experiment is difficult because introducing the magnetic flux and adiabatically controlling the periodic potential are difficult, recent experiments show that the Thouless pumping can be realized in ultracold atoms [4,5].

In a theoretical point of view, the Thouless pumping is a useful theoretical technique for detecting the topological invariant. In previous studies, the Thouless pumping in the quantum Hall system was numerically studied, and it was shown that the charge pumping continuously occurs from $t = 0$ (t represents time) and it reaches the quantized value at $t = T$ (T is the time interval during which the magnetization increases by Φ_0) in the adiabatic limit [6,7]. In quantum Hall systems, the total charge pumping is expressed by the topological invariant as follows [8,9]:

$$\Delta N(t = T) = N_{\mathrm{L}}(t = T) - N_{\mathrm{R}}(t = T) = 2\mathcal{C}, \qquad (1)$$

where $N_{\mathrm{L}}(t)$ [$N_{\mathrm{R}}(t)$] denotes the number of electrons distributed on the left side (right side) of the system and $\mathcal{C}$ is the topological invariant called the Chern number that takes integer values ($\mathcal{C} = 0, \pm 1, \pm 2, \dots$).

In the conventional ways for calculating the topological invariants, it is necessary to define the Bloch wave functions [10]. Although such definitions are useful for noninteracting systems with translational invariance, they are not directly used for nonperiodic systems such as disordered systems. In the Thouless pumping, by solving the time-dependent Schrödinger equations, it is easy to calculate the topological invariant even for disordered systems through the quantized charge pumping. We note that the Thouless pumping may be useful for detecting the topological invariant in correlated electron systems [11].

In this paper, by using the real-time evolution, we apply the Thouless pumping to Weyl semimetals where the quantized charge pumping also occurs [12–16]. We note that Weyl semimetals were recently found in inversion symmetry-broken systems such as TaAs [17–20] and time-reversal symmetry-broken systems (magnetic Weyl semimetals) such as Mn_3Sn [21,22], Heusler alloys [23,24], $Co_3Sn_2S_2$ [25–28], and $Sr_{1-y}Mn_{1-z}Sb_2$ [29]. Because magnetic Weyl semimetals can be constructed by stacking two-dimensional quantum anomalous Hall (QAH) systems (see Fig. 2), the Hall conductivity is quantized as follows:

$$\sigma_{xy} = \frac{e^2}{h}\frac{\Delta k}{2\pi}, \qquad (2)$$

where Δk is the distance between two Weyl points. By performing the Thouless pumping in the Weyl semimetal, it is expected that the charge pumping is also quantized as follows:

$$\Delta N = 2\Delta k \frac{L_z}{2\pi}, \qquad (3)$$

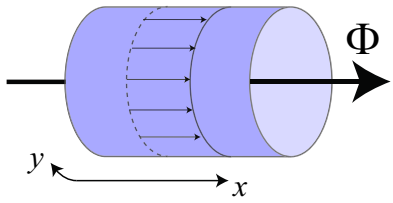

FIG. 1. Schematic picture of Laughlin's gedanken experiment in the quantum Hall system. By introducing flux Φ (equivalently, introducing electric field in the y direction), charge pumping occurs in the x direction.

where L_z is the length of the system in the z direction. In Weyl semimetals, however, the charge gap is zero, and it is nontrivial whether the Thouless pumping gives the quantized charge pumping for gapless systems or not. In this work, we show that quantized charge pumping occurs in the adiabatic limit. This result indicates that the Thouless pumping is useful even when the bulk charge gap is absent.

We also examine the effects of the disorder on the Thouless pumping and find that the charge pumping is robust against the small disorder and it increases in the intermediate-disorder region. These behaviors are consistent with previous studies [31–33]. This indicates that the Thouless pumping also works well for disordered systems.

This paper is organized as follows: In Sec. II A, we introduce model Hamiltonians for describing the Weyl semimetal and explain the algorithms for solving the time-dependent Schrödinger equation in Sec. II B. Although the algorithms are explained in the literature [34–37], to make our paper self-contained, we detail how to efficiently solve the time-dependent Schrödinger equations. In Sec. III A, we show the results of the Thouless pumping for the clean limit and at zero doping. Then, we examine the disorder effects in Sec. III B. We also examine the doping effects in Sec. III C and show that the Thouless pumping occurs for the finite-doping case; that is, a remnant of the quantization can be detected. Finally, Sec. IV is devoted to the summary.

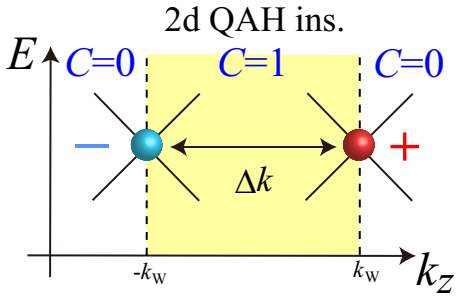

FIG. 2. Schematic picture of the Weyl points in the momentum space. The positions of the Weyl points are denoted by $\pm k_{\rm W}$. Signs of monopole charges [30] at the Weyl points are represented by $+$ and $-$. Inside the Weyl point ($-k_{\rm W} \leqslant k_z \leqslant k_{\rm W}$), the Chern number is nontrivial ($\mathcal{C} = 1$), while it is trivial outside the Weyl points ($\mathcal{C} = 0$). The Hall conductivity in the Weyl semimetal is given by $\sigma_{xy} = \frac{e^2}{h}\frac{\Delta k}{2\pi}$.

II. MODEL AND METHOD

A. Lattice model for Weyl semimetals

The Hamiltonian used in this study is given by

$$H_{\rm W} = \sum_{\nu=x,y,z} H_\nu + H_{\rm diag}, \tag{4}$$

$$H_\nu = \sum_j h_{\nu,j}, \tag{5}$$

$$h_{\nu,j} = c^\dagger_{j+\vec{e}_\nu} T_\nu c_j + {\rm H.c.}, \tag{6}$$

$$H_{\rm diag} = (2t_{\rm hop} - m)\sum_j c^\dagger_j \sigma_z c_j + \sum_j \epsilon_j c^\dagger_j \sigma_0 c_j, \tag{7}$$

$$\epsilon_j \in [-W/2, W/2], \tag{8}$$

where $c^\dagger_j$ (c_j) represents the two-component fermion creation (annihilation) operator defined on a site j on the three-dimensional cubic lattice spanned by three orthogonal unit vectors $\vec{e}_{\nu=x,y,z}$. The matrices T_ν are defined as

$$T_x = t_{\rm hop}(-\sigma_z + i\sigma_x)/2, \tag{9}$$

$$T_y = t_{\rm hop}(-\sigma_z + i\sigma_y)/2, \tag{10}$$

$$T_z = -t_{\rm hop}\sigma_z/2, \tag{11}$$

where

$$\sigma_x = \begin{pmatrix} 0 & 1 \\ 1 & 0 \end{pmatrix}, \quad \sigma_y = \begin{pmatrix} 0 & -i \\ i & 0 \end{pmatrix}, \quad \sigma_z = \begin{pmatrix} 1 & 0 \\ 0 & -1 \end{pmatrix}. \tag{12}$$

Throughout this paper, we take the amplitude of the hopping transfer $t_{\rm hop} = 1$ as a unit of the energy scale.

The band structure of the Hamiltonian is given by

$$E_{\rm W} = \pm[(\sin k_x)^2 + (\sin k_y)^2 + (2 - m - \cos k_x - \cos k_y - \cos k_z)^2]^{1/2}. \tag{13}$$

From this band structure, we can show that the Weyl points are located at $(0, 0, k_{\rm W} = \pm\cos^{-1}(-m))$ for $|m| < 1$. Around the Weyl points, the dispersions are given as

$$E_{\rm W} \sim \pm\left(k_x^2 + k_y^2 + \tilde{k}_z^2\right)^{1/2}, \tag{14}$$

where $\tilde{k}_z = \sqrt{1-m^2}[k_z - \cos^{-1}(-m)]$. We note that the Weyl semimetal is constructed by stacking the two-dimensional QAH insulators. As shown in Fig. 2, the Chern number becomes nontrivial between the two Weyl points, and it becomes trivial outside the Weyl points. Thus, the quantized Hall conductivity is proportional to $\Delta k = 2k_{\rm W}$.

To perform the Thouless pumping, we introduce the time-dependent vector potentials as follows:

$$T_y(t) = e^{iA_y(t)}T_y, \tag{15}$$

$$A_y(t) = \frac{2\pi t}{L_y T}. \tag{16}$$

By introducing $A_y(t)$ in the y direction, the charge pumping in the x direction occurs if the Hall conductivity is finite.

B. Method for solving the time-dependent Schrödinger equations

To perform the Thouless pumping, we explicitly solve the time-dependent Schrödinger equation defined as

$$i\frac{\partial\,|\phi(t)\rangle}{\partial t} = H_{\rm W}\,|\phi(t)\rangle\,. \tag{17}$$

Here, $|\phi(t)\rangle$ is a single Slater determinant given by

$$|\phi(t)\rangle = \prod_{n=1}^{N_{\rm e}}\left(\sum_{i=0}^{N_{\rm s}-1}\Phi_{ni}(t)c_i^\dagger\right)|0\rangle\,, \tag{18}$$

where $N_{\rm e}$ is the number of particles, $N_{\rm s}$ is the number of sites, and $\Phi_{ni}(t)$ denotes the coefficient of the Slater determinant. By discretizing the time and multiplying the time evolution operator $U(t+\Delta t,t)$ by the wave functions at each discretized time step, we can solve the time-dependent Schrödinger equations as follows:

$$|\phi(t+\Delta t)\rangle = U(t+\Delta t,t)\,|\phi(t)\rangle\,, \tag{19}$$

$$U(t+\Delta t,t) = \mathcal{T}\left\{\exp\left[-i\int_t^{t+\Delta t}H_W(s)ds\right]\right\}, \tag{20}$$

where $\mathcal{T}$ it the time ordering operator.

One simple way to solve the time-dependent Schrödinger equation is given by

$$|\phi(t+\Delta t)\rangle \sim \exp\left[-i\Delta t H_W(t)\right]|\phi(t)\rangle. \tag{21}$$

Here, we approximate $U(t+\Delta,t)$ as $\exp\left[-i\Delta t H_W(t)\right]$, and we denote the coefficients of the Hamiltonian as $\tilde{H}_W$, i.e., $H_W(t) = c^\dagger \tilde{H}_W(t)c$. By diagonalizing $\tilde{H}_W(t)$ at each time step, we obtain the solutions as follows:

$$e^{-i\Delta t c^\dagger \tilde{H}_W(t)c}\,|\phi(t)\rangle = \prod_{n=1}^{N_{\rm e}}\left[\sum_{i=0}^{N_{\rm s}-1}\Phi_{ni}(t+\Delta t)c_i^\dagger\right]|0\rangle\,, \tag{22}$$

$$\Phi_{ni}(t+\Delta t) = \sum_{\alpha j}\Phi_{nj}(t)e^{-i\Delta t\lambda_\alpha}(V^\dagger)_{\alpha j}V_{i\alpha}, \tag{23}$$

$$V^\dagger \tilde{H}_W(t)V = {\rm diag}(\lambda_0,\lambda_1,\ldots,\lambda_{2N_{\rm s}-1}). \tag{24}$$

Because this method requires the diagonalization of the Hamiltonian at each step, the computational costs are large. To reduce the costs, we decompose the time-evolution operator by using the Suzuki-Trotter decomposition [34–36]. In this method, because the diagonalization of the full Hamiltonian is necessary only for preparing the initial wave functions, computational cost is drastically reduced.

From here, we explain the outline of the method. Since the cubic lattice is bipartite, we decompose the nearest-neighbor hopping terms in the Hamiltonian into two parts as follows:

$$H_\nu = H_{\nu,e} + H_{\nu,o}, \tag{25}$$

$$H_{\nu,e} = h_{\nu,0} + h_{\nu,2} + \cdots\,, \tag{26}$$

$$H_{\nu,o} = h_{\nu,1} + h_{\nu,3} + \cdots\,, \tag{27}$$

where $h_{\nu,2n\,(2n+1)}$ contains hopping terms between sites on $\nu = 2n\,(2n+1)$ and those on $\nu = 2n+1\,(2n+2)$ for $\nu = x,y,z$. We note that each component of the Hamiltonian can be described as

$$h_{\nu,i} = \begin{pmatrix}c_i^\dagger & c_{i+\vec{e}_\nu}^\dagger\end{pmatrix}K_\nu\begin{pmatrix}c_i\\ c_{i+\vec{e}_\nu}\end{pmatrix}. \tag{28}$$

For example, K_x is given by

$$K_x = \frac{1}{2}\begin{pmatrix}0&0&-1&-i\\0&0&-i&1\\-1&i&0&0\\i&1&0&0\end{pmatrix}. \tag{29}$$

Because $h_{\nu,2j}$ are commutable with each other ($h_{\nu,2j+1}$ are also commutable with each other), it is easy to decompose $e^{H_{\nu,e}}$ and $e^{H_{\nu,o}}$ as follows:

$$e^{H_{\nu,e}} = e^{h_{\nu,0}}\times e^{h_{\nu,2}}\times\cdots\,, \tag{30}$$

$$e^{H_{\nu,o}} = e^{h_{\nu,1}}\times e^{h_{\nu,3}}\times\cdots\,. \tag{31}$$

From this relation, by just diagonalizing $h_{\nu,i}$, whose matrix size is 4×4, we can perform the real-time evolutions.

Because $H_{\nu,e}$ and $H_{\nu,o}$ are not commutable, we use the fourth-order Suzuki-Trotter decomposition [34], whose general form is by

$$e^{\eta(A_1+\cdots+A_q)} = S(\eta p)S(\eta(1-2p))S(\eta p) + O(\eta^5), \tag{32}$$

$$\begin{aligned}S(\eta) = {}& e^{\eta A_1/2}e^{\eta A_2/2}\cdots e^{\eta A_{q-1}/2}e^{\eta A_q}\\ &\times e^{\eta A_{q-1}/2}\cdots e^{\eta A_1/2},\end{aligned} \tag{33}$$

$$p = (2-2^{1/3})^{-1}, \tag{34}$$

where η is the c number and A_q denotes the matrix. By using the formula, we can decompose $e^{\eta H_{\rm W}}$ as follows:

$$e^{\eta H_{\rm W}} = S(\eta p)S(\eta(1-2p))S(\eta p), \tag{35}$$

$$S(\eta) = S_0(\eta)e^{\eta H_{\rm diag}}S_1(\eta), \tag{36}$$

$$\begin{aligned}S_0(\eta) = {}& e^{\eta H_{x,e}/2}e^{\eta H_{x,o}/2}e^{\eta H_{y,e}/2}e^{\eta H_{y,o}/2}\\ &\times e^{\eta H_{z,e}/2}e^{\eta H_{t}nz,o/2},\\ S_1(\eta) = {}& e^{\eta H_{z,o}/2}e^{\eta H_{z,e}/2}e^{\eta H_{y,o}/2}e^{\eta H_{y,e}/2}\\ &\times e^{\eta H_{x,o}/2}e^{\eta H_{x,e}/2}.\end{aligned} \tag{37}$$

If the Hamiltonian is not the time-dependent one, this formula has fourth-order precision. For the time-dependent Hamiltonian, the time-evolution operator is defined by using the *superoperator* $\tilde{\mathcal{T}}$ as follows [35,36]:

$$U(t+\Delta t,t) = \exp\left\{\Delta t[-iH(t)+\tilde{\mathcal{T}}]\right\}, \tag{38}$$

$$F(t)e^{\Delta t\tilde{\mathcal{T}}}G(t) = F(t+\Delta t)G(t). \tag{39}$$

Here, F and G are arbitrary functions. We note that the superoperator $\tilde{\mathcal{T}}$ acts on only the operators on its left. By using this formula, we decompose U as follows:

$$\begin{aligned}U(t+\Delta t,t) = {}& S(-i\Delta t p, t+(1-p/2)\Delta t)\\ &\times S(-i\Delta t(1-2p), t+p\Delta t/2)\\ &\times S(-i\Delta t p, t+p\Delta t/2)+O(\Delta t^5),\end{aligned} \tag{40}$$

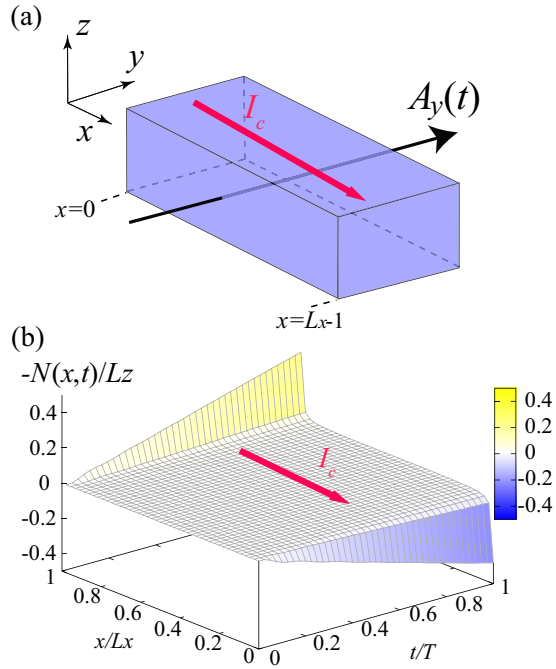

FIG. 3. (a) Schematic illustration of the geometry used in this study. We take the open boundary condition in the x direction and the periodic boundary conditions in the y and z directions. The employed geometry is given by $L = L_x = 2L_y = 2L_z$. We introduce $A_y(t)$ in the y direction, and charge pumping occurs in the x direction. (b) Time dependence of the charge distribution $N(x,t)$ in the x direction. We take $m = 0$, $T = 20$, $W = 0$, and $L = 44$. The charge pumping occurs around the edges in the x direction by introducing $A_y(t)$.

where time-dependent S is defined as

$$S(\eta,t) = S_0(\eta,t)e^{\eta H_{\rm diag}}S_1(\eta,t), \tag{41}$$

$$\begin{aligned} S_0(\eta,t) &= e^{\eta H_{x,e}/2}e^{\eta H_{x,o}/2}e^{\eta H_{y,e}(t)/2} \\ &\quad\times e^{\eta H_{y,o}(t)/2}e^{\eta H_{z,e}/2}e^{\eta H_{z,o}/2}, \\ S_1(\eta,t) &= e^{\eta H_{z,o}/2}e^{\eta H_{z,e}/2}e^{\eta H_{y,o}(t)/2} \\ &\quad\times e^{\eta H_{y,e}(t)/2}e^{\eta H_{x,o}/2}e^{\eta H_{x,e}/2}. \end{aligned} \tag{42}$$

We note that superoperator $\tilde{\mathcal{T}}$ operates all the left-side operators. By using Eq. (40), we perform the real-time evolution.

III. RESULTS

A. Thouless pumping in Weyl semimetals

In Fig. 3(a), we show a setup of the Thouless pumping for a Weyl semimetal. The system size is given by $N_s = L_x \times L_y \times L_z$, and we employ the rectangle geometry given by $L = L_x = 2L_y = 2L_z$. In the x (y and z) direction, we employ the open (periodic) boundary condition. By applying the vector potentials in the y direction [Eq. (16)], it is expected that the quantized charge pumping in the x direction occurs. We take $\Delta t = 0.02$ and $m = 0$ in this paper.

In this setup, we perform the Thouless pumping, i.e., solve the time-dependent Schrödinger equations, and obtain $|\phi(t)\rangle$. From $|\phi(t)\rangle$, we calculate the time-dependent charge distribution in the x direction, which is defined as

$$\begin{aligned} N(x,t) = \sum_{y,z}[&\langle\phi(t)|\, c^\dagger_{x,y,z}c_{x,y,z}\,|\phi(t)\rangle \\ &- \langle\phi(0)|\, c^\dagger_{x,y,z}c_{x,y,z}\,|\phi(0)\rangle]. \end{aligned} \tag{43}$$

As shown in Fig. 3(b), by introducing the vector potentials in the y direction, the charge pumping in the x direction occurs; that is, $N(x,t)$ becomes positive around $x = 0$, while it becomes negative around $x = L_x - 1$. This result shows that the pumped charge is mainly induced at the edges in the clean limit.

At $t = T$, the total pumped charge is expected to be quantized for sufficiently large T. The total pumped charge is defined as

$$\Delta N(t) = \sum_{0\leqslant x<L_x/2} N(x,t) - \sum_{L_x/2\leqslant x<L_x} N(x,t). \tag{44}$$

We show $\Delta N(t)$ for several different system sizes in Fig. 4(a). We find that $\Delta N(t)$ monotonically increases as a function of t, and it nearly becomes L_z at $t = T$. This is consistent with the topological properties of the Weyl semimetals; that is, the Hall conductivity is quantized as $\sigma_{xy} = (e^2/2\pi h)\Delta k$, and the corresponding charge pumping is given by $\Delta N = (\Delta k/\pi)L_z$. This result indicates that the Thouless pumping works well even when the systems have no bulk gaps.

To examine when the Thouless pumping can be regarded as an adiabatic process, we calculate the unit time T dependence of the charge pumping. In Fig. 4(b), we show the T dependence of $\Delta N(t = T)$ for several different system sizes. For small T ($T < 1$), the speed of introducing $A_y(t)$ is too fast to change the electronic states in the Weyl semimetals. Thus, for $T < 1$, the Thouless pumping is nonadiabatic, and the pumped charge is not quantized. By increasing T, for $T \geqslant 10$, the pumped charge is quantized except for small oscillations. This result indicates that the Thouless pumping can be regarded as an adiabatic process for $T \geqslant 10$. Thus, we take $T = 20$ in the remainder of this paper. We note that the typical timescale does not significantly change for the weak-disorder region, but it becomes large for the strong-disorder region. Nevertheless, we note that the charge pumping at $T = 20$ can be regarded as adiabatic pumping in the relevant disorder region.

We note that Laughlin's argument or Thouless's argument requires the existence of a bulk charge gap for the quantized charge pumping. The Weyl semimetal has no bulk charge gap, and it is unclear whether the Thouless pumping works well or not. By comparing it with the T dependence in the two-dimensional QAH insulator as shown in Fig. 4(b), we find that the T dependence of the pumped charge for the Weyl semimetal is basically the same as that of the QAH insulator. This result clearly shows that the Thouless pumping works well for detecting the topological invariant even when the systems have no bulk gap.

B. Effects of disorders

We examine how the disorder affects the charge pumping in the Weyl semimetal. In general, the topological property is robust against the perturbations because the topological

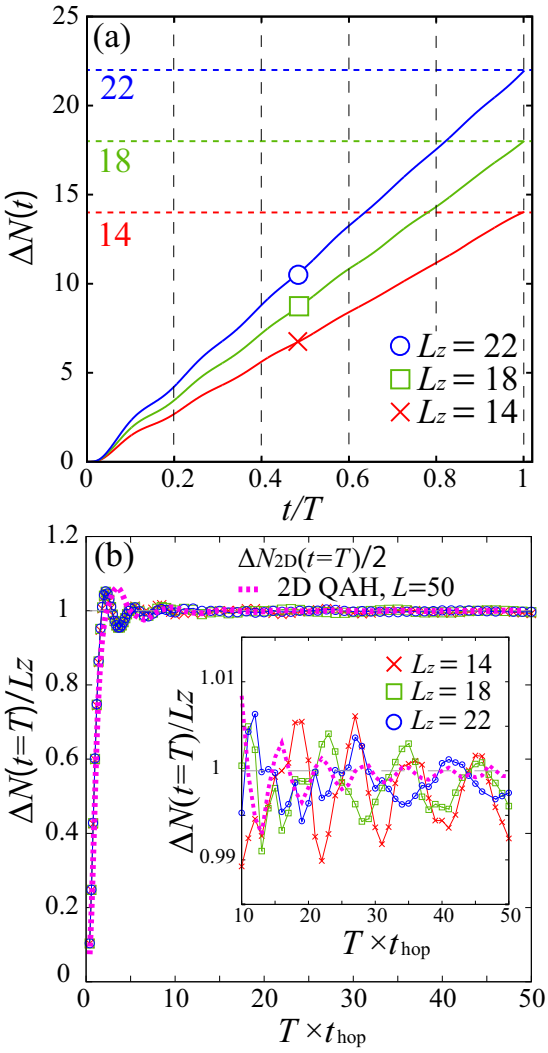

FIG. 4. (a) System size dependence of the charge pumping as a function of time. We take $T = 20$, $W = 0$, and $m = 0$. The charge pumping $t = T$ is quantized as $\Delta N(t = T) = 2\Delta k \frac{L_z}{2\pi}$, which is proportional to L_z. (b) T dependence of the charge pumping. For small T, because introducing $A_y(t)$ is not adiabatic, the charge pumping is not quantized. For comparison, we also show the T dependence of the charge pumping for the two-dimensional QAH insulator $N_{2D}(t = T)$, where the bulk gap exists. Details of the two-dimensional QAH insulator are shown in the Appendix. For $T \geqslant 10$, the charge pumping is nearly quantized for both systems except for small oscillations. In the inset, we show an enlarged figure for $T \geqslant 10$. In contrast to the gapped system [see the inset of Fig. 9(b)], for the Weyl semimetal, we find that the small but finite oscillations remain even for larger T. These remaining oscillations may originate from the gapless nature of the Weyl semimetal.

property cannot be changed by the perturbations unless the energy scale of the perturbations reaches that of the charge gap. For a Weyl semimetal, it is, however, unclear whether the topological property remains or not because the bulk charge gap is zero in a Weyl semimetal. Several theoretical studies, however, showed that topological properties in Weyl semimetals are robust against small disorder [31–33,38]. We examine whether the Thouless pumping can reproduce the

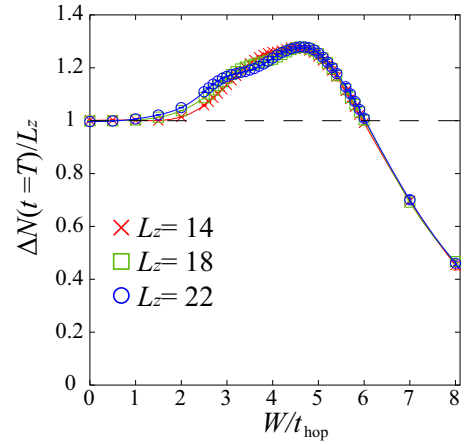

FIG. 5. Disorder dependence of the pumped charge at $t = T$. We take $T = 20$ and $m = 0$.

results of the previous studies. We note that we do not consider the rare region effects [39–41] in this paper.

In Fig. 5, we show the disorder dependence of total charge pumping $\Delta N(t = T)$. We find that overall behaviors are consistent with previous studies [31–33,38]: a plateau for small disorder ($W \lesssim 1$), enhanced charge pumping in the intermediate-disorder ($W \sim 3$) region, and a decrease of the charge pumping in the strong-disorder region ($W \gtrsim 4.5$). We note that enhancement of the charge pumping is not observed in the two-dimensional QAH insulator, as shown in the Appendix.

To examine how the pumped charge is enhanced by the disorder, we analyze the real-space dependence of the pumped charge. In Fig. 6, we show the charge distribution at $t = T$ for several different strengths of the disorders. Because the charge pumping mainly occurs around the edges ($x \sim 0, L_x - 1$), we enlarge the shaded region in Fig. 6(a) and plot the x dependence of the pumped charge measured from the clean limit $[\Delta\tilde{N}(x, t) = \Delta N(x, t, W) - \Delta N(x, t, W = 0)]$ in Fig. 6(b).

For small disorder ($W = 2$), we find that the disorder mainly changes the pumping around the edges, and it does not affect the pumping inside the systems. This enhancement for small disorder can be explained by the mass renormalization effects [31–33,38]; that is, disorder increases the mass term m and widens the length of Fermi arcs. By further increasing the strengths of the disorders, we find that the pumped charge begins to penetrate into the systems. This behavior can be explained as follows: For the strong-disorder region, the Fermi arcs at the surfaces begin to mix with the bulk states. This mixing induces the penetration of the Fermi arcs inside the systems; that is, Fermi arcs begin to have finite width in the x direction and induce the charge pumping inside of the systems. This is the reason why the pumped charge is enhanced by the disorder.

C. Effects of doping

In this section, we examine the effects of doping on the charge pumping in the Weyl semimetal. First, we examine whether the adiabatic limit of the charge pumping exists for finite doping where the finite density of states exists. In

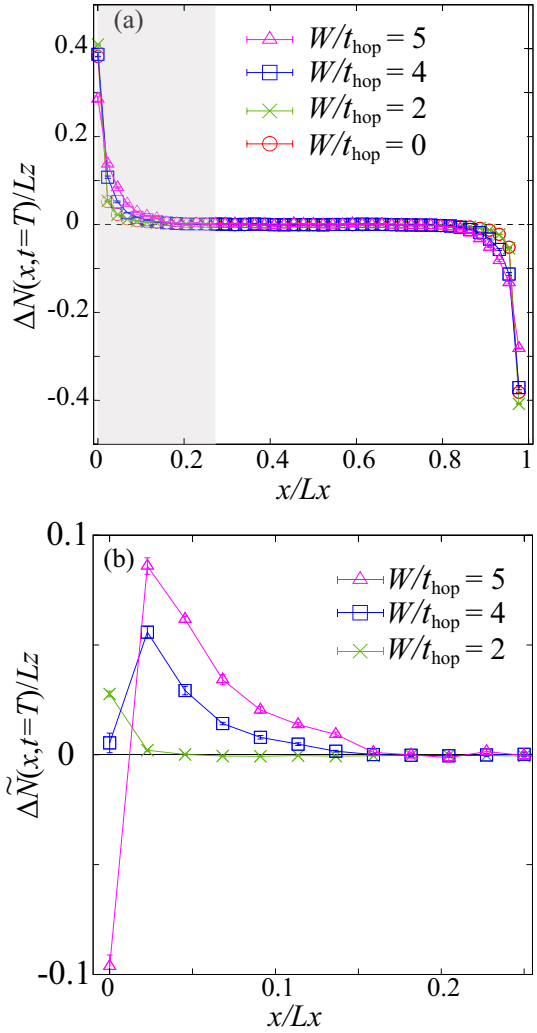

FIG. 6. (a) Charge pumping in the presence of the disorder. We plot $\Delta N(x,t)/L_z$ at $t=T$ for several different strengths of disorder. To estimate the errors of the realizations of the disorder, we take five different realizations and regard the standard errors as error bars. We take $L=44$ and $m=0$. (b) Pumped charge measured from the clean limit $[\Delta\tilde{N}(x,t=T)]$ in the shaded region in (a). By increasing the strength of the disorder, we find that the pumped charges penetrate into the inside of the system.

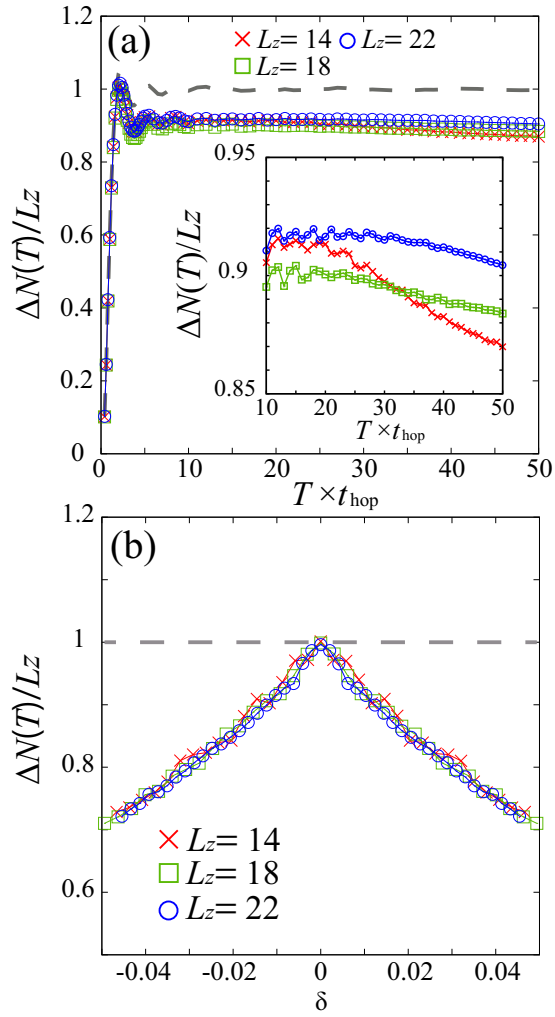

FIG. 7. (a) T dependence of the charge pumping $\Delta N(t=T)/L_z$ at finite doping $\delta=0.01$. We take $m=0$. For comparison, we plot the result at zero doping with dashed lines. In the inset, we show an enlarged figure for $T\geqslant 10$. (b) Doping dependence of charge pumping for $T=20$. Charge pumping monotonically decreases with doping.

Fig. 7(a), we show the T dependence of the pumped charge. At small T ($T\leqslant 1$), i.e., in the nonadiabatic process, the T dependence of the pumped charge is the same as that of zero doping. Here, the doping rate is defined as $\delta=\Delta N/N_s$, where ΔN is the number of electrons measured from half filling, i.e., $\Delta N=N_e-N_s$. In the nonadiabatic region, because the electrons move too fast, the low-energy structures of the systems such as Fermi surfaces do not affect the charge pumping. This is the reason why the pumped charges do not change in the nonadiabatic region.

By taking larger T, we find that the T dependence of the charge pumping is basically the same as that of the nondoping case; that is, the large oscillations seen for small T ($T\leqslant 5$) are suppressed, and the pumped charge seems to converge to a constant for $T\leqslant 20$. However, as shown in the inset in Fig. 7(a), it slightly decreases for $T\geqslant 20$, and there is considerable system-size dependence. From the available data, it is difficult to identify whether the origin of the decrease is the finite-size effects or not, and it is also difficult to accurately estimate the converged pumped charge in the long-time and bulk limit for the doped case. Nevertheless, as we show later, the pumped charge around $T=20$ can capture the essence of the finite-doping effects on the charge pumping and can be useful for detecting the remnant of the quantized charge pumping at zero doping. Thus, to examine the doping effects, we use the pumped charge at $T=20$ as a simple estimation of the converged value.

In Fig. 7(b), we show the doping dependence of the pumped charge for $T=20$. We find that the pumped charge monotonically decreases for electron and hole doping except for slight oscillations found in small system sizes. This result shows that doping in Weyl semimetals continuously lowers the pumped charge from its quantized values at zero doping. We note that the changes in the pumped charge are induced

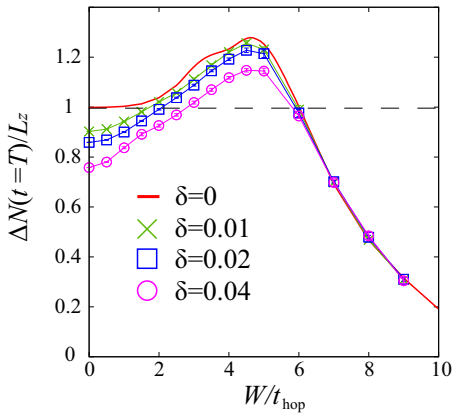

FIG. 8. Disorder W dependence of pumped charge at finite doping. We take $T = 20$ and $m = 0$.

by the Berry curvature in nonlinear dispersions because the Berry curvature in linear dispersions around the Weyl points does not contribute to the pumped charge. We note that the saddle points around the zero doping are located at $E_{\rm saddle} = \pm t_{\rm hop}$ and the corresponding doping rate is given by $\delta_{\rm saddle} \sim \pm 0.065$.

We examine the disorder effects of the Thouless pumping at finite dopings. In Fig. 8, we plot the disorder W dependence of the pumped charge for several different doping rates. At finite-doping rates, quantization at zero doping is absent; the pumped charge monotonically increases as a function of the disorder strength W. By further increasing the disorder, the pumped charge has peaks around $W \sim 4.5$ as in the case of zero doping. The robustness of the peak structure against the finite-doping rates is a characteristic feature of Weyl semimetals. In the strong-disorder region ($W \geqslant 6$), charge pumping does not depend on the doping rates because the Fermi surfaces are completely smeared out in this region.

IV. SUMMARY

To summarize, we introduced a lattice model for Weyl semimetals in Sec. II A and detailed the methods for solving the time-dependent Schrödinger equations by using the fourth-order Suzuki-Trotter decomposition in Sec. II B. Although the time-dependent Schrödinger equations can be solved by performing the diagonalization of the Hamiltonian at each time step, the numerical cost of diagonalization is large, and that method cannot be applied to large systems. The Suzuki-Trotter decomposition method does not require the diagonalization of the full Hamiltonian at each time step, and numerical cost is dramatically reduced. By using this method, we can perform the Thouless pumping up to the order of 10^4-site systems.

In Sec. III A, we showed the results of the Thouless pumping for the clean limit and zero doping. Although a Weyl semimetal does not have a bulk charge gap, we found that the Thouless pumping works well for detecting the topological quantization of Weyl semimetals. By examining the unit time T dependence of the charge pumping, we confirmed that the adiabatic charge pumping occurs for larger T, typically $T \geqslant 20$.

In Sec. III B, we examined the disorder effects on the Thouless pumping. We note that the Thouless pumping itself can be applied to disorder systems without changing the method because we just solve the time-dependent Schrödinger equations in real space. As a result, we have shown that the quantized pumped charge is robust against small disorder. We have also shown that the pumped charge increases by increasing the disorder for the intermediate strength of disorder. These behaviors are consistent with previous studies [31–33,38]. This shows that the usefulness of the Thouless pumping for detecting the topological properties in disordered systems.

We have found that the charge pumping has a large system size dependence around $W \sim 3$, as shown in Fig. 5, where the transition between Weyl semimetals and a diffusive metal is pointed out in the literature [32]. Thus, this system size dependence may be related to the transition into the diffusive metal. In this study, the available system size was limited, and it was difficult to perform accurate finite-size scaling for detecting the signatures of the phase transitions. Systematic calculations for determining the phase transitions is left for future studies.

In Sec. III C, we examined the effects of doping into the Weyl semimetals. For finite-doping rates, we found that the pumped charge slightly decreases for larger T and it is difficult to accurately estimate the pumped charge in the adiabatic limit. In this paper, we simply used the pumped charge at $T = 20$ as a rough estimation of the adiabatic pumping. It is left for future studies to accurately estimate the pumped charge in the adiabatic limit by performing calculations for larger system sizes and larger T. By using the pumped charge at $T = 20$, we showed that the remnant of the quantized pumped charge can be detected for finite-doping rates. We also showed that the pumped charge is also enhanced by increasing the disorders for finite-doping rates. The peak positions of the charge pumping under disorder do not largely depend on the doping rates.

Our results show that the Thouless pumping is a useful theoretical tool for detecting the topological properties even for gapless systems such as Weyl semimetals. This method is also applicable to doped systems and can capture the remnant of the topological properties of the systems through the charge pumping. Because the Thouless pumping requires only the real-time evolution of the ground-state wave functions, it can be applied to correlated electron systems, where it is difficult to obtain full eigenvectors. For the one-dimensional system, the Thouless pumping for the correlated system was studied in detail [11]. Recent studies [42–44] showed that it is possible to perform accurate real-time evolutions of the wave functions in correlated quantum many-body systems based on the time-dependent variation principles [45]. Studies in this direction are intriguing challenges for clarifying the nature of the correlated topological systems in more than one dimension, and our detailed study of the Thouless pumping presented in this paper offers a firm basis for such advanced studies.

ACKNOWLEDGMENTS

Our calculation was partly carried out at the Supercomputer Center, Institute for Solid State Physics, University

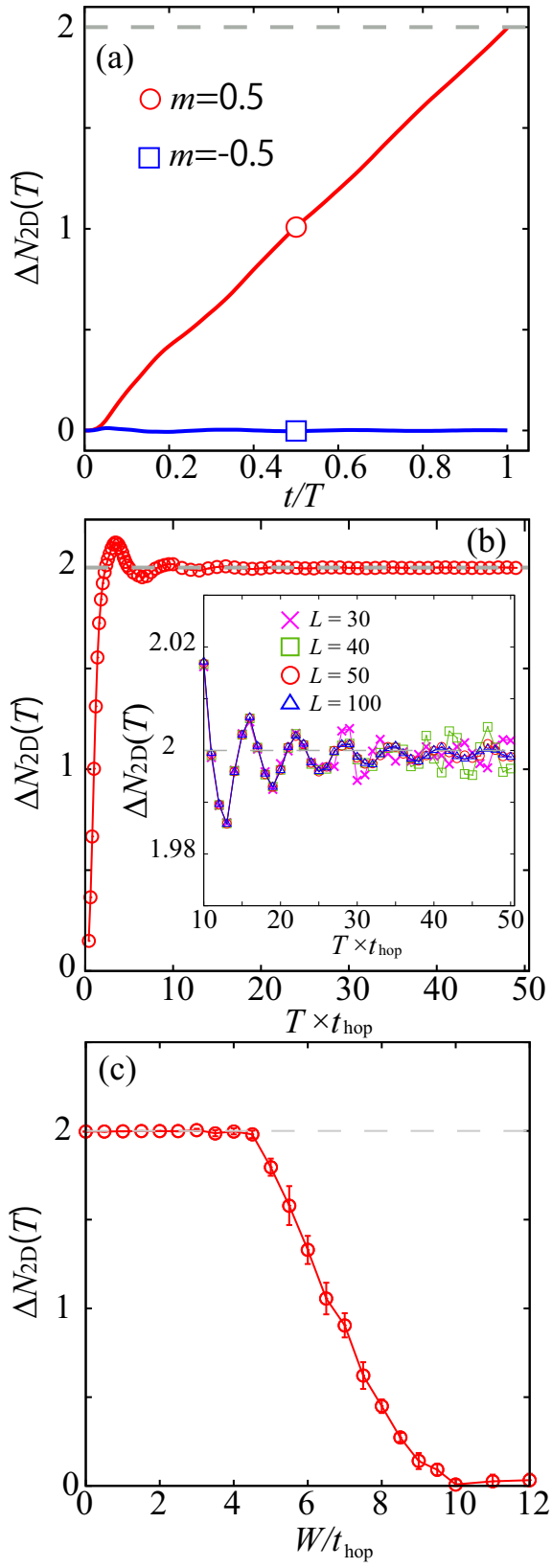

FIG. 9. (a) Thouless pumping for the Chern insulator ($m = 0.5$) and trivial insulator ($m = -0.5$). We take $L = 50$ and $T = 20$. (b) T dependence of charge pumping for $L = 50$ and $m = 0.5$. In the inset, we show an enlarged figure for $T \geqslant 10$. In the QAH systems, we find that the oscillations in the pumped charge become smaller for larger T. (c) Disorder dependence of the pumped charge.

of Tokyo. This work was supported by JSPS KAKENHI (Grants No. JP15H05854, No. JP16H06345, No. JP16K17746, No. JP17K05485, No. JP17K17604, and No. JP19K03739). T.M. thanks K.-I. Imura for useful discussions on real-time evolutions. We also thank K. Kobayashi for useful discussions on the disordered magnetic Weyl semimetal. T.M. was also supported by Building of Consortia for the Development of Human Resources in Science and Technology from MEXT of Japan. This work was also supported by the Japan Society for the Promotion of Science and JST CREST (JPMJCR18T2).

APPENDIX: THOULESS PUMPING IN TWO-DIMENSIONAL CHERN INSULATORS

Here, we show the results of the Thouless pumping for two-dimensional quantum anomalous Hall (QAH) insulators. By simply ignoring the z dependence of the Weyl Hamiltonians, we can obtain the lattice Hamiltonian for the two-dimensional QAH insulators as follows:

$$H_{\rm QAH} = \sum_{\nu=x,y} H_\nu + H_{\rm diag}, \tag{A1}$$

$$H_{\rm diag} = (2-m)\sum_j c_j^\dagger \sigma_z c_j + \sum_j \epsilon_j c_j^\dagger \sigma_0 c_j, \tag{A2}$$

$$\epsilon_j \in [-W/2, W/2]. \tag{A3}$$

For $m > 0$, we obtain the QAH insulator with $\mathcal{C} = 1$, and a trivial insulator appears for $m < 0$. We consider $L = L_x = L_y$ systems, and the pumped charge is given by

$$\Delta N_{\rm 2D}(t) = \sum_{0\leqslant x<L_x/2,y} N(x,y,t) - \sum_{L_x/2\leqslant x<L_x,y} N(x,y,t). \tag{A4}$$

We note that the charge pumping is quantized as follows:

$$\Delta N_{\rm 2D}(t = T) = 2\mathcal{C}, \tag{A5}$$

where $\mathcal{C}$ is the Chern number.

In Fig. 9(a), we show the results of the Thouless pumping for $m = 0.5$ and $m = -0.5$. In the topologically trivial insulator ($m = -0.5$), the charge pumping does not occur, while the charge pumping is quantized for $m = 0.5$. Because the Chern number is 1 in this system, the quantized charge pumping becomes 2.

We show the T dependence of $\Delta N_{\rm 2D}(T)$ in Fig. 9(b). Similar to Weyl semimetals, although the oscillation occurs for small T ($T \leqslant 10$), the charge pumping converges to the quantized value. In QAH insulators, we show only the results for $L = 50$ because size effects are small.

We show the disorder dependence of $\Delta N_{\rm 2D}(T)$ in Fig. 9(c). In contrast to Weyl semimetals, the charge pumping does not have peak structures. For $W \leqslant 5$, the pumped charge is quantized, and it begins to decrease for $W \geqslant 5$. This result indicates that the characteristic enhanced charge pumping in Weyl semimetals is induced by their gapless nature.

[1] K. v. Klitzing, G. Dorda, and M. Pepper, Phys. Rev. Lett. **45**, 494 (1980).
[2] R. B. Laughlin, Phys. Rev. B **23**, 5632 (1981).
[3] D. J. Thouless, Phys. Rev. B **27**, 6083 (1983).
[4] S. Nakajima, T. Tomita, S. Taie, T. Ichinose, H. Ozawa, L. Wang, M. Troyer, and Y. Takahashi, Nat. Phys. **12**, 296 (2016).
[5] M. Lohse, C. Schweizer, O. Zilberberg, M. Aidelsburger, and I. Bloch, Nat. Phys. **12**, 350 (2016).
[6] I. Maruyama and Y. Hatsugai, J. Phys.: Conf. Ser. **150**, 022055 (2009).
[7] Y. Hatsugai and T. Fukui, Phys. Rev. B **94**, 041102(R) (2016).
[8] D. J. Thouless, M. Kohmoto, M. P. Nightingale, and M. den Nijs, Phys. Rev. Lett. **49**, 405 (1982).
[9] M. Kohmoto, Ann. Phys. (NY) **160**, 343 (1985).
[10] S. Ryu, A. P. Schnyder, A. Furusaki, and A. W. Ludwig, New J. Phys. **12**, 065010 (2010).
[11] M. Nakagawa, T. Yoshida, R. Peters, and N. Kawakami, Phys. Rev. B **98**, 115147 (2018).
[12] R. Shindou and N. Nagaosa, Phys. Rev. Lett. **87**, 116801 (2001).
[13] S. Murakami, New J. Phys. **9**, 356 (2007).
[14] X. Wan, A. M. Turner, A. Vishwanath, and S. Y. Savrasov, Phys. Rev. B **83**, 205101 (2011).
[15] A. A. Burkov and L. Balents, Phys. Rev. Lett. **107**, 127205 (2011).
[16] A. Burkov, Annu. Rev. Condens. Matter Phys. **9**, 359 (2018).
[17] S.-Y. Xu, I. Belopolski, N. Alidoust, M. Neupane, G. Bian, C. Zhang, R. Sankar, G. Chang, Z. Yuan, C.-C. Lee *et al.*, Science **349**, 613 (2015).
[18] B. Q. Lv, H. M. Weng, B. B. Fu, X. P. Wang, H. Miao, J. Ma, P. Richard, X. C. Huang, L. X. Zhao, G. F. Chen *et al.*, Phys. Rev. X **5**, 031013 (2015).
[19] B. Lv, N. Xu, H. Weng, J. Ma, P. Richard, X. Huang, L. Zhao, G. Chen, C. Matt, F. Bisti *et al.*, Nat. Phys. **11**, 724 (2015).
[20] L. Yang, Z. Liu, Y. Sun, H. Peng, H. Yang, T. Zhang, B. Zhou, Y. Zhang, Y. Guo, M. Rahn *et al.*, Nat. Phys. **11**, 728 (2015).
[21] K. Kuroda, T. Tomita, M.-T. Suzuki, C. Bareille, A. Nugroho, P. Goswami, M. Ochi, M. Ikhlas, M. Nakayama, S. Akebi *et al.*, Nat. Mater. **16**, 1090 (2017).
[22] N. Ito and K. Nomura, J. Phys. Soc. Jpn. **86**, 063703 (2017).
[23] Z. Wang, M. G. Vergniory, S. Kushwaha, M. Hirschberger, E. V. Chulkov, A. Ernst, N. P. Ong, R. J. Cava, and B. A. Bernevig, Phys. Rev. Lett. **117**, 236401 (2016).
[24] G. Chang, S.-Y. Xu, H. Zheng, B. Singh, C.-H. Hsu, G. Bian, N. Alidoust, I. Belopolski, D. S. Sanchez, S. Zhang *et al.*, Sci. Rep. **6**, 38839 (2016).
[25] E. Liu, Y. Sun, N. Kumar, L. Muechler, A. Sun, L. Jiao, S.-Y. Yang, D. Liu, A. Liang, Q. Xu *et al.*, Nat. Phys. **14**, 1125 (2018).
[26] Q. Xu, E. Liu, W. Shi, L. Muechler, J. Gayles, C. Felser, and Y. Sun, Phys. Rev. B **97**, 235416 (2018).
[27] Q. Wang, Y. Xu, R. Lou, Z. Liu, M. Li, Y. Huang, D. Shen, H. Weng, S. Wang, and H. Lei, Nat. Commun. **9**, 3681 (2018).
[28] A. Ozawa and K. Nomura, arXiv:1904.08148.
[29] J. Liu, J. Hu, Q. Zhang, D. Graf, H. B. Cao, S. Radmanesh, D. Adams, Y. Zhu, G. Cheng, X. Liu *et al.*, Nat. Mater. **16**, 905 (2017).
[30] M. Hirayama, R. Okugawa, S. Ishibashi, S. Murakami, and T. Miyake, Phys. Rev. Lett. **114**, 206401 (2015).
[31] C.-Z. Chen, J. Song, H. Jiang, Q.-f. Sun, Z. Wang, and X. C. Xie, Phys. Rev. Lett. **115**, 246603 (2015).
[32] H. Shapourian and T. L. Hughes, Phys. Rev. B **93**, 075108 (2016).
[33] Y. Takane, J. Phys. Soc. Jpn. **85**, 124711 (2016).
[34] M. Suzuki, Phys. Lett. A **146**, 319 (1990).
[35] M. Suzuki, Proc. Jpn. Acad., Ser. B **69**, 161 (1993).
[36] M. Suzuki, Commun. Math. Phys. **163**, 491 (1994).
[37] T. Nakanishi, T. Ohtsuki, and T. Kawarabayashi, J. Phys. Soc. Jpn. **66**, 949 (1997).
[38] S. Liu, T. Ohtsuki, and R. Shindou, Phys. Rev. Lett. **116**, 066401 (2016).
[39] R. Nandkishore, D. A. Huse, and S. L. Sondhi, Phys. Rev. B **89**, 245110 (2014).
[40] J. H. Pixley, D. A. Huse, and S. Das Sarma, Phys. Rev. X **6**, 021042 (2016).
[41] J. Lee, J. H. Pixley, and J. D. Sau, Phys. Rev. B **98**, 245109 (2018).
[42] J. Haegeman, J. I. Cirac, T. J. Osborne, I. Pižorn, H. Verschelde, and F. Verstraete, Phys. Rev. Lett. **107**, 070601 (2011).
[43] G. Carleo, F. Becca, M. Schiró, and M. Fabrizio, Sci. Rep. **2**, 243 (2012).
[44] K. Ido, T. Ohgoe, and M. Imada, Phys. Rev. B **92**, 245106 (2015).
[45] A. McLachlan, Mol. Phys. **8**, 39 (1964).